Journal of Physics: Condensed Matter

PAPER

Phase difference dependence of output power in synchronized stacked spin Hall nano-oscillators

To cite this article: Kang Doo Hyung and Shin Mincheol 2018 *J. Phys.: Condens. Matter* **30** 284001

View the article online for updates and enhancements.

Related content

- Synchronization and chaos in spin-transfer-torque nano-oscillators coupled via a high-speed operational amplifier
C Sanid and S Murugesh
- CMOS-compatible spintronic devices: a review
Alexander Makarov, Thomas Windbacher, Viktor Sverdlov et al.
- Magnetic vortex oscillators
Gino Hrkac, Paul S Keatley, Matthew T Bryan et al.

IOP ebooks™

Bringing you innovative digital publishing with leading voices to create your essential collection of books in STEM research.

Start exploring the collection - download the first chapter of every title for free.

This content was downloaded from IP address 143.248.37.172 on 18/12/2018 at 06:24

IOP Publishing Journal of Physics: Condensed Matter
J. Phys.: Condens. Matter **30** (2018) 284001 (8pp) https://doi.org/10.1088/1361-648X/aac864

Phase difference dependence of output power in synchronized stacked spin Hall nano-oscillators

Kang Doo Hyung and Shin Mincheol

Department of Electronic Engineering, Korea Advanced Institute of Science and Technology, Daejeon 34141, Republic of Korea

E-mail: ppassionata@kaist.ac.kr and mshin@kaist.ac.kr

Received 21 November 2017, revised 21 May 2018
Accepted for publication 29 May 2018
Published 19 June 2018

Abstract

Synchronization between stacked spin Hall nano-oscillators (SHNO), attributed to the spin Hall effect and anisotropic magnetoresistance effect, was studied by numerical calculations. In order to obtain the synchronized state of the SHNOs, we considered the magneto-dipolar field, which was calculated in the rectangular prism. We revealed that the output power depended on the distance between the SHNOs, as the phase difference between the SHNOs depended on the coupling strength. For $N = 3$ (number of SHNOs), we investigated the phase difference by considering the influence of the coupling strength of all magnetic layers. Furthermore, we observed that the output power increased with the number of SHNOs in the synchronization system.

Keywords: spin torque nano oscillators, spin Hall effect, spin Hall nano-oscillators, synchronization, magneto-dipolar coupling

(Some figures may appear in colour only in the online journal)

1. Introduction

An electronic control of magnetic properties of magnetic materials offers various advantages including a development of devices with a high level of integration [1, 2]. In spin transfer torque devices, the spin torque, attributed to exchange interactions between the spin of conduction electrons and local magnetization of the free layer, provides an ability for an electronic control of the magnetization of the free layer [3, 4]. The spin torque effect in nanoscale magnetic devices such as magnetic tunnel junctions induces magnetization switching [5–10] and magnetization precession [11–13].

Spin torque nano-oscillators (STNOs) have attracted significant research interests over the past few decades owing to their potentials for applications as devices in the GHz frequency band [14–20]. The STNO is composed of an f/s/p structure, where f is the free layer, which is a thin ferromagnetic layer, s is the spacer, and p is the pinned layer, which is a thick ferromagnetic layer. When a DC electrical current flows through the STNO, a spin current is generated owing to the spin filtering of the pinned layer, and induces a magnetization precession of the free layer. The combination of the magnetization precession in the free layer and giant magnetoresistance or tunnel magnetoresistance effect induces voltage oscillations.

Recently, spin Hall nano-oscillator (SHNO) composed of a heavy-metal/ferromagnetic-material (H/F) structure has attracted a significant attention as a novel type of spin oscillator [21–27]. Compared with STNOs, SHNOs can be more easily nanofabricated, can be operated at a lower DC current, and exhibit suppressed damping, which prevents magnetization precession [28, 29]. When a longitudinal charge current flows through the SHNO, a transverse pure spin current is generated owing to the spin Hall effect (SHE) in the heavy metal, attributed to the spin–orbit interactions. The generated pure spin current flows to the ferromagnetic material and induces a magnetization precession owing to the exerted torque on the magnetization. In this case, the combination of magnetization precession and anisotropic magnetoresistance (AMR) effect leads to the voltage oscillations [21, 26].

 © 2018 IOP Publishing Ltd Printed in the UK

In the experimental study, bulk and edge modes are exhibited in the nanowire SHNO [26]. However, in the micromagnetic study by Siracusano *et al*, spatially uniform mode in the entire region of the nanowire SHNO is excited in certain applied magnetic field and current ranges due to the uniform Oersted field in the whole nanowire SHNO [30]. In a conventional current-perpendicular-plane spin torque oscillator, a non-uniform Orested field that induces a spatially inhomogeneous magnetization excitation, such as a vortex state, is developed in the radial direction. On the contrary, in the nanowire SHNO, the uniform Oersted field is displayed within the entire ferromagnet, which enables single mode magnetization excitation.

For practical applications of STNOs and SHNOs, it is necessary to increase the output power and reduce the linewidth. The synchronization between STNOs has been extensively studied, as if N STNOs are in-phase synchronized, the output power increases N^2 times, and the linewidth reduces to $1/N^2$ [31], where N is the total number of STNOs. Kaka *et al* and Mancoff *et al* independently reported a synchronization in a double-point-contact device [32, 33]. They demonstrated the increased output power and reduced linewidth during the synchronization. By employing the nonlinear auto-oscillator model, Slavin and Tiberkevich showed that the locking range of synchronization depends on the coupling strength between the auto-oscillators [34]. Using numerical calculations, Person *et al* and Zhou *et al* showed that the locking range can be extended using a phase shifter, as a capacitor, in the electrical coupling system [35, 36]. The synchronization induced by magneto-dipolar coupling between STNOs was investigated by Chen *et al* [37]. Recently, using micromagnetic simulations, Puliafito demonstrated that the output power of the synchronized state in a double-point-contact STNO depends on the phase difference between two STNOs [38]. However, the correlation between the coupling strength and phase difference in the magnetic coupling system for $N > 2$ has not been studied.

In this study, we investigate the synchronization of stacked nanowire SHNOs with magneto-dipolar coupling. In order to obtain the magneto-dipolar field, we calculate the demagnetization tensor in the rectangular prism. As the output power of synchronized SHNOs depends on the phase difference between the SHNOs, which in turn depends on the coupling strength, we investigate the output power as a function of the distance between the SHNOs [34]. For $N = 3$, we investigate the correlation between the phase difference and coupling strength of all of the magnetic layers. For this purpose, we calculate the ratio between the coupling strengths of the next-nearest-neighbor and nearest-neighbor layers. Furthermore, we perform calculations to investigate whether the output power increases N^2 times when N SHNOs are in a synchronized state. Although a magnetic uniform mode is developed in the low current region in Siracusano's investigation [30], we use the macrospin simulation method to calculate the synchronization between SHNOs under the assumption that the single mode can be achieved in the high current region, which induces the out-of-plane (OOP) precession. In a spin-torque oscillator system, a magnetic field along the out-of-plane direction, such as a demagnetization field, induces an OOP precession in the high current region, even if the external field is applied along the in-plane direction [31]. The investigated nanowire SHNOs have strong demagnetization fields. Thus, uniform OOP precession in the nanowire SHNOs can be expected because of the uniform Oersted field. In addition, Chen *et al* showed that the parameter range, including synchronization range and coupling strength, of the synchronized state induced by the magnetic coupling is almost same for both the macrospin and micromagnetic simulation, in the spin valve system [39].

2. Model and description

2.1. Electrical model of output power

We follow the procedure employed by Puliafito *et al* [38] and consider two SHNOs, which utilize the SHE and AMR effect. The output power of the synchronized state between the two SHNOs can be expressed as:

$$\begin{aligned} P_{\mathrm{L}} = {} & P_{\mathrm{L1}} + P_{\mathrm{L2}} + \frac{4}{3}\sqrt{P_{\mathrm{L1}}P_{\mathrm{L2}}} \\ & + \frac{2}{3}\sqrt{P_{\mathrm{L1}}P_{\mathrm{L2}}}\big[\langle \cos 2[(\omega_1+\omega_2)t + (\phi_1+\phi_2)]\rangle \\ & + \langle \cos 2[(\omega_1-\omega_2)t + (\phi_1-\phi_2)]\rangle\big], \end{aligned} \tag{1}$$

where P_{L1} (P_{L2}) is the output power of the $\mathrm{SHNO_1}$ ($\mathrm{SHNO_2}$), ω_1 (ω_2) is the frequency of the $\mathrm{SHNO_1}$ ($\mathrm{SHNO_2}$), and ϕ_1 (ϕ_2) is the phase of the $\mathrm{SHNO_1}$ ($\mathrm{SHNO_2}$). If $\omega_1 \neq \omega_2$ (non-synchronization), the output power is $P_{\mathrm{L}} = P_{\mathrm{L1}} + P_{\mathrm{L2}} + \frac{4}{3}\sqrt{P_{\mathrm{L1}}P_{\mathrm{L2}}}$. If $\omega_1 = \omega_2$ and $\phi_1 \neq \phi_2$ (out-of-phase synchronization), the output power is:

$$P_{\mathrm{L}} = P_{\mathrm{L1}} + P_{\mathrm{L2}} + \frac{4}{3}\sqrt{P_{\mathrm{L1}}P_{\mathrm{L2}}} + \frac{2}{3}\sqrt{P_{\mathrm{L1}}P_{\mathrm{L2}}}\big(\cos 2(\phi_1-\phi_2)\big). \tag{2}$$

Equation (2) indicates that the output power of the synchronized SHNOs depends on the phase difference between the two SHNOs. If the phase difference ($\Delta\phi$) satisfies $45^\circ < \Delta\phi < 135^\circ$, the output power is reduced even though a synchronization exists, owing to a destructive interference in this region. If $\omega_1 = \omega_2$ and $\phi_1 = \phi_2$ (in-phase synchronization), the output power is:

$$P_{\mathrm{L}} = P_{\mathrm{L1}} + P_{\mathrm{L2}} + 2.0\sqrt{P_{\mathrm{L1}}P_{\mathrm{L2}}}. \tag{3}$$

When $P_{\mathrm{L1}} = P_{\mathrm{L2}}$, we obtain $P_{\mathrm{L}} = 4P_{\mathrm{L1}}$.

2.2. Simulation model and description

As a model system, we consider SHNOs connected in parallel, as shown in figures 1(a) and (b). Each SHNO consists of an F/H/insulator-(In) structure. When a DC current flows through the SHNO, the SHE generates a spin current, $\vec{J}_s$, in the heavy metal layer. The spin current injected into the ferromagnetic layer exerts a spin torque on the magnetization of the ferromagnet and induces a magnetization precession. The magnetization excitation and AMR effect lead to oscillations of the resistance of the SHNO. The insulator is introduced to block

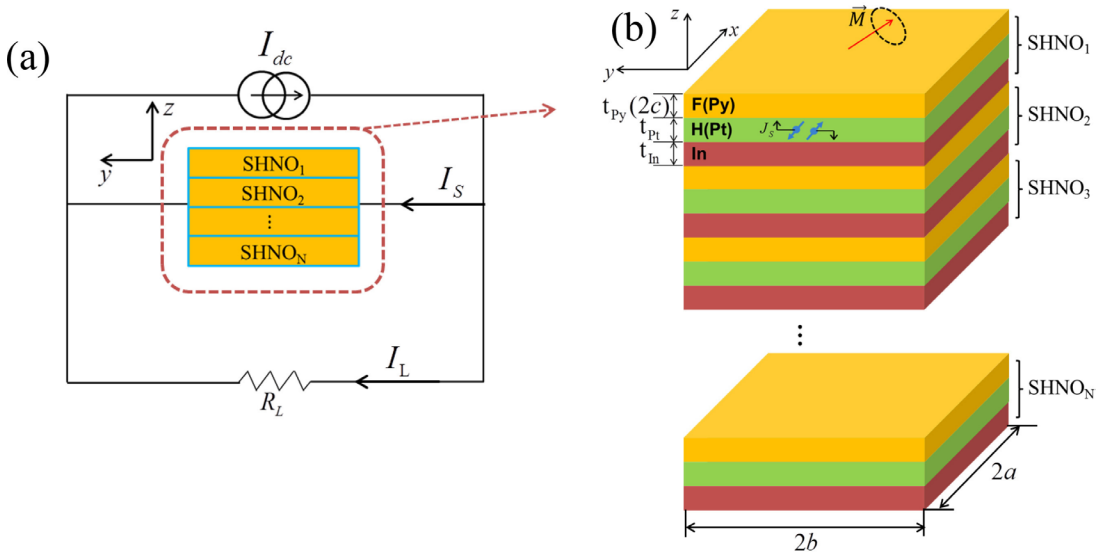

Figure 1. (a) Circuit diagram of N stacked SHNOs connected in parallel, where I_{dc} is the DC current, and I_S and I_L are the currents flowing through the SHNOs and load resistance, respectively. (b) Detailed schematic of the part outlined by the red dotted line in figure (a). The SHNO is composed of an F(Py)/H(Pt)/In trilayer; $t_{Py} = 2c$, t_{Pt}, and t_{In} are the thicknesses of the Py, Pt, and insulator layers, respectively. $2a$ and $2b$ are the width and length of the SHNOs, respectively. In this model, the magneto-dipolar interaction is the dominant contribution to the coupling between the SHNOs.

the inflow of spin current from the neighboring SHNO in the stacked SHNOs. In this model, Platinum (Pt) and Permalloy (Py) are used as the heavy metal and ferromagnetic material, respectively.

In order to investigate the magnetization dynamics in the Py layer, we use the Landau–Lifshitz–Gilbert–Slonczewski equation: [3, 4]

$$\frac{\mathrm{d}\hat{m}_j}{\mathrm{d}t} = -\gamma \hat{m}_j \times \vec{H}_{\mathrm{eff},j} + \alpha \hat{m}_j \times \frac{\mathrm{d}\hat{m}_j}{\mathrm{d}t} + \gamma \frac{\hbar}{2e\mu_0 M_S t_{Py}} J_s \hat{m}_j \times (\hat{\sigma} \times \hat{m}_j), \tag{4}$$

where $\hat{m}_j$ is the unit vector of the magnetization of the jth Py layer ($j = 1, 2, \cdots, N$), $\hat{\sigma}$ is the unit vector of the injected spin moment, γ is the gyromagnetic ratio, α is the Gilbert damping constant, M_s is the saturation magnetization of Py, t_{Py} is the thickness of the Py layer, $J_s\hbar/2e$ is the spin current density injected into the Py layer, and $\vec{H}_{\mathrm{eff},j}$ is the effective magnetic field exerted on the jth Py layer, which can be expressed as:

$$\vec{H}_{\mathrm{eff},j} = H_{\mathrm{ext}}\hat{x} + H_k(\hat{m}_j \cdot \hat{x})\hat{x} + \vec{H}_{j,\mathrm{Am}} + \sum_{k=1}^{N} \vec{H}_{j,k}, \tag{5}$$

where H_{ext} is the applied magnetic field, H_k is the magneto-crystalline anisotropy field of the Py layer, $\hat{x}$ is the unit vector along the x-axis, and $\vec{H}_{j,\mathrm{Am}}$ is the Oersted field created by the current, exerted on the jth Py layer. Although the magnitude of the Oersted field depends on the x- and z- coordinates in the Py layer, we consider a volume-averaged Oersted field of the jth Py layer in the macrospin model. $\vec{H}_{j,k}$ is the magneto-dipolar field, which is created by the kth Py layer, exerted on the jth Py layer. As only the excitation of a spatially uniform mode is considered, we calculate a magneto-dipolar field averaged over the volume V_j of the jth Py layer [40, 41]:

$$\vec{H}_{j,k} = \frac{1}{V_j}\int_{V_j} \vec{H}_k(\vec{r}_j)\mathrm{d}V_j, \tag{6}$$

where $\vec{H}_k(\vec{r}_j)$ is the spatially non-uniform magneto-dipolar field created by the magnetization distribution, $\vec{M}_k$, of the kth Py layer; it can be expressed as:

$$\vec{H}_k(\vec{r}) = -\mathbb{N}_k(\vec{r}) \cdot \vec{M}_k, \tag{7}$$

where $\mathbb{N}_k(\vec{r})$ is the point-function demagnetization tensor [40, 42, 43]. Using equations (6) and (7), we obtain the volume-averaged demagnetization tensor as:

$$\mathbb{N}_{j,k}(\vec{r}) = \frac{1}{V_j}\int_{V_j} \mathbb{N}_k(\vec{r}_j)\mathrm{d}\vec{r}_j, \tag{8}$$

where $\mathbb{N}_{j,j}$ ($j = k$) is the self-demagnetization tensor, which is the normal demagnetization tensor in the jth Py layer, while $\mathbb{N}_{j,k}(j \neq k)$ is the cross-demagnetization tensor representing the dipolar interactions between the jth and kth Py layers.

The calculations of the demagnetization tensors for a rectangular prism are comprehensively described in our previous study [44]. In this study, we briefly introduce the calculation procedures. The x,x and x,y components of the point-function demagnetization tensor are expressed in SI units as [40, 42, 44, 45]:

$$N_k^{x,x}(\vec{r}_k) = \frac{1}{4\pi}\sum_{l,m,n=1}^{2} \arctan\left[\frac{(b-y_m)(c-z_n)}{(a-x_l)D(x_l,y_m,z_n)}\right], \tag{9}$$

$$N_k^{x,y}(\vec{r}_k) = -\frac{1}{4\pi}\sum_{l,m=1}^{2}(-1)^{l+m}\Big(\ln\left[(c-z_1)+D(x_l,y_m,z_1)\right] - \ln\left[-(c-z_2)+D(x_l,y_m,z_2)\right]\Big), \tag{10}$$

respectively, where $N_k^{x,x}$ and $N_k^{x,y}$ are the x,x and x,y components of the point-function demagnetization tensor, (x_1, y_1, z_1) and (x_2, y_2, z_2) denote $(+x, +y, +z)$ and $(-x, -y, -z)$, respectively,

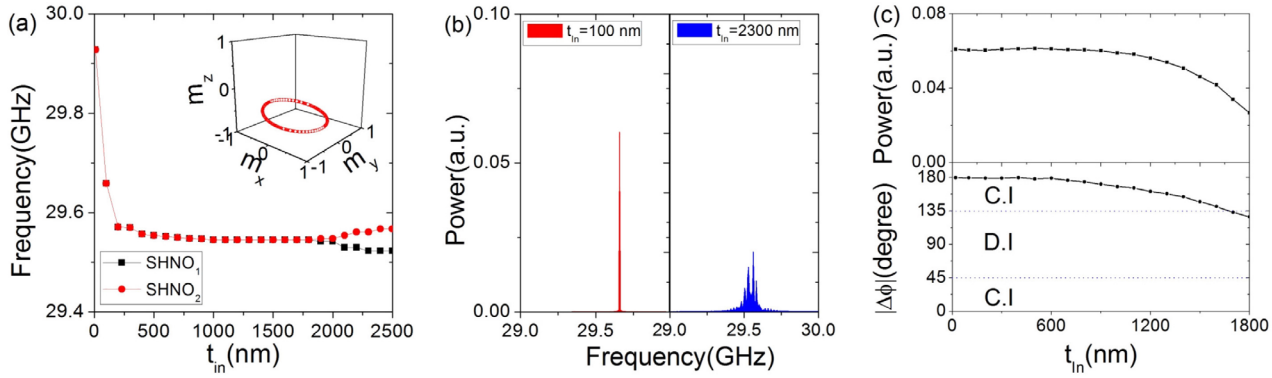

Figure 2. (a) Dependence of the synchronization between the two SHNOs as a function of t_{In}. For $t_{\mathrm{In}} \leqslant 1800$ nm, the frequencies of the two SHNOs are identical. The inset shows the orbit of the magnetization of the SHNO_1 for $t_{\mathrm{In}} = 100$ nm. (b) Output powers of the SHNOs for a synchronized (left panel) and non-synchronized (right panel) states at $t_{\mathrm{In}} = 100$ nm (left panel) and 2300 nm (right panel). (c) Output power and phase difference $|\Delta\phi|$ of the SHNOs as a function of t_{In} at $I_{\mathrm{dc}} = 24.0$ mA.

and $D(x_l, y_m, z_n) = \sqrt{(a-x_l)^2 + (b-y_m)^2 + (c-z_n)^2}$. The other components of the demagnetization tensor elements can be derived from equations (9) and (10) by permutations of the coordinates.

Using equations (8) and (9), and integrating by substitution with new variables, $X = (a - x_l)$, $Y = (b - y_m)$, $Z = (c - z_n)$, and $D = \sqrt{X^2 + Y^2 + Z^2}$, we can express the x,x component of the volume-averaged self-demagnetization tensor as:

$$N_{k,k}^{x,x} = \frac{1}{4\pi abc}\big[g(2a,2b,2c) - g(0,2b,2c) - g(2a,0,2c) - g(2a,2b,0) + g(0,0,2c) + g(0,2b,0) + g(2a,0,0) - g(0,0,0)\big], \tag{11}$$

where $g(X,Y,Z)$ can be expressed as:

$$g(X,Y,Z) = XYZ\arctan\left[\frac{YZ}{XD} + \frac{1}{4}Y(X^2 - Z^2)\ln\left(\frac{D+Y}{D-Y}\right) + \frac{1}{4}Z(X^2 - Y^2)\ln\left(\frac{D+Z}{D-Z}\right) + \frac{1}{6}(Y^2 + Z^2 - 2X^2)D\right]. \tag{12}$$

The other diagonal components and all off-diagonal components of the self- and cross-demagnetization tensors can be easily obtained with the same approach; all off-diagonal components are zero.

Further, we calculate the current passing through the SHNOs and load resistance in the circuit. By employing the Kirchhoff's law for the parallel circuit in figure 1(a), we obtain the current passing through SHNO_1, SHNO_2, $\cdots$, SHNO_N, and R_{L}:

$$I_{si} = \frac{R_{\mathrm{L}}\prod_{j=1,j\neq i}^{N} R_j I_{\mathrm{dc}}}{R_{\mathrm{L}}\left(\prod_{j=1,j\neq 1}^{N} R_j + \prod_{j=1,j\neq 2}^{N} R_j + \cdots + \prod_{j=1,j\neq N}^{N} R_j\right) + \prod_{j=1}^{N} R_j}$$

$$I_{\mathrm{L}} = \frac{\prod_{j=1}^{N} R_j I_{\mathrm{dc}}}{R_{\mathrm{L}}\left(\prod_{j=1,j\neq 1}^{N} R_j + \prod_{j=1,j\neq 2}^{N} R_j + \cdots + \prod_{j=1,j\neq N}^{N} R_j\right) + \prod_{j=1}^{N} R_j}$$

$$I_{i,\mathrm{Pt}} = \frac{R_{i,\mathrm{Py}} I_{si}}{R_{i,\mathrm{Py}}} + R_{i,\mathrm{Pt}}, \tag{13}$$

where I_{si}, I_{L}, and $I_{i,\mathrm{Pt}}$ are the currents passing through the ith SHNO ($i = 1, 2, \cdots, N$), load resistance, and ith Pt layer, respectively. R_i ($i = 1, 2, \cdots, N$) is the resistance of the SHNOs, which can be expressed as:

$$R_i = \frac{R_{i,\mathrm{Py}} R_{i,\mathrm{Pt}}}{R_{i,\mathrm{Py}} + R_{i,\mathrm{Pt}}}, \tag{14}$$

where $R_{i,\mathrm{Py}}$ ($R_{i,\mathrm{Pt}}$) is the resistance of the Py (Pt) layer of the ith SHNO. The resistivity of the Py layer can be expressed as [46]:

$$\rho_{i,\mathrm{Py}} = \rho_0 + \kappa\rho_0 \cos^2\theta(t), \tag{15}$$

where $\rho_{i,\mathrm{Py}}$ is the resistivity of the ith Py layer, ρ_0 is the resistivity when the direction of the current is perpendicular to the magnetization of the Py layer, κ is the AMR ratio, and $\theta(t)$ is the angle between the direction of the current and magnetization at the time moment t.

The spin current injected into the Py layer can be obtain using the spin Hall angle, $\theta_{\mathrm{SH}} = J_{\mathrm{S}}/J_{\mathrm{Pt}}$, which generally characterizes the SHE, where J_{Pt} is the current density flowing through the Pt layer.

3. Results and discussion

The parameters used in our simulation to describe the Pt/Py bilayer SHNO are [21, 26, 47]: $\alpha = 0.007$, $\gamma = 1.85 \times 10^{11}$ Hz T^{-1}, $2a = 200$ nm, $2b = 6$ μm, $2c(= t_{\mathrm{Py}}) = 2$ nm, $t_{\mathrm{Pt}} = 6$ nm, $H_{\mathrm{ext}} = 0.1$ T, $H_k = 0.005$ T, $\rho_{\mathrm{Pt}} = 0.2$ $\mu\Omega$m, $\rho_0 = 0.45$ $\mu\Omega$m, $\kappa = 0.01$, $M_s = 0.804$ T, and $R_{\mathrm{L}} = 50$ Ω. In our simulation, we vary the thickness of the In layer, t_{In}, to obtain different distances between the Py layers. Different natural frequencies of the SHNOs are obtained by an assumption of SHNOs with different spin Hall angles, i.e. $\theta_{\mathrm{SH}}, i = 0.08 + (0.0003 \times i - 0.0003)$. OOP precession is considered in this study as the synchronization range of the OOP precession is significantly wider than that of the in-plane (IP) precession [31, 47]. In addition, it is assumed that all SHNOs are equal except for the different spin Hall angle.

Further, we discuss the synchronization of stacked SHNOs with magneto-dipolar coupling. Figure 2 shows the synchronization between two SHNOs. The frequency variation as a function of t_{In} for $I_{\mathrm{dc}} = 24$ mA is shown in figure 2(a), where the black and red dotted lines represent the frequencies of the SHNO_1 and SHNO_2, respectively. The generated

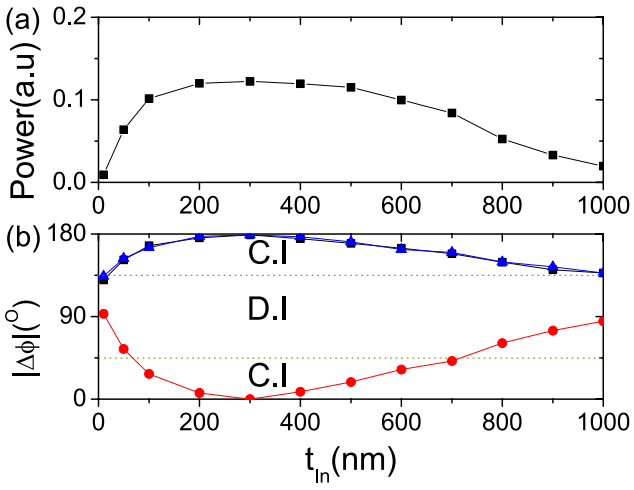

Figure 3. Dependences of the (a) output power and (b) phase difference as a function of the distance between the SHNOs for $N = 3$ and $I_{dc} = 24.0$ mA, where the black, red, and blue dotted lines in (b) represent $|\Delta\phi_{2,1}|$, $|\Delta\phi_{3,1}|$, and $|\Delta\phi_{3,2}|$, respectively.

frequencies of the $SHNO_1$ and $SHNO_2$ become similar with the decrease of t_{In}, and in the region of $t_{In} \leqslant 1800$ nm the two frequencies coincide, which indicates the synchronization between the two SHNOs. The inset in figure 2(a) shows the trajectory of the magnetization of the $SHNO_1$ for $t_{In} = 100$ nm, which corresponds to an OOP precession. In the region of the synchronized state, with the decrease of t_{In}, the frequency increases as the magneto-dipolar field becomes larger. Figure 2(b) shows the output powers of a microwave on the load resistance at $t_{In} = 100$ nm and $t_{In} = 2300$ nm for $I_{dc} = 24$ mA, presented in the frequency domain using a fast Fourier transform. In the left panel of figure 2(b), only one peak exists at $f = 29.66$ GHz, which implies a synchronization of the SHNOs. On the other hand, in the right panel, two peaks are observed at $f = 29.53$ GHz and $f = 29.56$ GHz, which indicates a non-synchronized state. Compared with the non-synchronized state, the synchronized state exhibits a larger output power. The output power of the SHNOs in the synchronized state depends on the phase difference ($\Delta\phi$) between the SHNOs [38]. According to Slavin and Tiberkevich, the phase difference between two auto-oscillators tends to be located in the out-of-phase region with the decrease of the coupling strength [34]. Figure 2(c) shows the dependence of the output power (upper panel) and $|\Delta\phi|$ (lower panel), where C. I. (D. I.) denotes a constructive (destructive) interference. As $|\Delta\phi|$ gradually decreases from 180° with the increase of t_{In}, the synchronized state increasingly deviates from the in-phase synchronization, and in addition, the output power decreases. Although $|\Delta\phi|$ corresponds to a constructive interference in the range of $t_{In} \leqslant 1600$ nm, the output power decreases in this range with the increase of t_{In} as the maximum output power is achieved at $|\Delta\phi| = 0°$ or $|\Delta\phi| = 180°$ (equation (2)).

Figures 3(a) and (b) show the output power and $|\Delta\phi|$, respectively, for $N = 3$ and $I_{dc} = 24$ mA as a function of t_{In}. For $N = 3$, three $|\Delta\phi|$ ($|\Delta\phi_{2,1}|$, $|\Delta\phi_{3,2}|$, and $|\Delta\phi_{3,1}|$) exist. As shown in figure 3(b), the $\Delta\phi$ between nearest layers ($|\Delta\phi_{2,1}|$ and $|\Delta\phi_{3,2}|$) exhibit a similar tendency, whereas the $|\Delta\phi|$ of the next-nearest layer ($|\Delta\phi_{3,1}|$) exhibits an opposite tendency compared with that of the nearest layer. With the increase of t_{In} to 200 nm, the output power rapidly increases; it is almost constant in the t_{In} range of 200–500 nm, and then it decreases rapidly for $t_{In} \geqslant 600$ nm, as shown in figure 3(a). In contrast to figure 2(c), the maximum output power is at $t_{In} = 300$ nm as an in-phase synchronization occurs for $t_{In} = 300$ nm.

The magneto-dipolar coupling is a dominant factor for the synchronization between the SHNOs in the presented model. In order to change the cross-demagnetization tensor, we change the width and length of the SHNO, while keeping constant its height and ratio between the length and width. In addition, we maintain the current density flowing through the SHNOs to provide the same spin current density as used in figure 3 to the Py layer. Figure 4(a) shows the output power as a function of t_{In} for different a at $N = 3$, where power(max) denotes the maximum value of the output power depending on t_{In}. The orange dotted line represents the boundary of power/power(max) = 0.95 in figure 4(a). We observed that the maximum output power appears at a smaller t_{In} with the decrease of a; for $a = 10, 40, 70$, and 100 nm, the maximum output power appears at $t_{In} = 50, 100, 200$, and 300 nm, respectively. In addition, the range of power/power(max)$\geqslant 0.95$ becomes broader with the increase of a. According to the auto-oscillator model, a larger coupling strength induces an in-phase synchronization between two oscillators [34]. In order to investigate the correlation between the magneto-dipolar coupling strength and t_{In} dependence of the output power in the synchronization of three SHNOs, we calculate the ratio between $N^{x,x}_{1,3}$ and $N^{x,x}_{1,2}$ as a function of t_{In} for different a. The x- component of the magneto-dipolar field is of importance for the synchronization between the SHNOs owing to its large amplitude, compared with those of the other two components [44]. As shown in figure 4(b), $N^{x,x}_{1,3}/N^{x,x}_{1,2}$ decreases with the increase of t_{In} for all values of a. We revealed that the power/power(max) is closely related to $N^{x,x}_{1,3}/N^{x,x}_{1,2}$; when power/power(max) is equal for different value of a, $N^{x,x}_{1,3}/N^{x,x}_{1,2}$ is similar for the different values of a. For example, as shown in figure 4(a), power/power(max) = 1 is observed at $t_{In} = 50, 100, 200$, and 300 nm for $a = 10, 40, 70$, and 100 nm, respectively. As shown in figure 4(b), $N^{x,x}_{1,3}/N^{x,x}_{1,2} = 0.24, 0.28, 0.27$, and 0.27 at $t_{In} = 50$ ($a = 10$ nm), 100 ($a = 40$ nm), 200 ($a = 70$ nm), and 300 ($a = 100$ nm), respectively. In addition, the region of power/power(max) > 0.95 in figure 4(a) corresponds to the $N^{x,x}_{1,3}/N^{x,x}_{1,2}$ range of $0.24 \sim 0.32$ (yellow dotted line) in figure 4(b).

Further, we calculate the output power for different thicknesses of insulator layers in different SHNOs at $N = 3$, i.e. $t_{In,1-2} \neq t_{In,2-3}$, where $t_{In,1-2}$ ($t_{In,2-3}$) is the thickness of the insulator layer between $SHNO_1$ ($SHNO_2$) and $SHNO_2$ ($SHNO_3$). Figure 5 shows the output power for $t_{In,2-3} = t_{In,1-2}$, $t_{In,2-3} = 1.01t_{In,1-2}$, $t_{In,2-3} = 1.05t_{In,1-2}$, and $t_{In,2-3} = 1.1t_{In,1-2}$ at $2a = 200$ nm, $2b = 6\,\mu$m, and $2c = 2$ nm. The maximum values of the output powers are almost identical and appear at $t_{In,1-2} = 300$ nm for all cases.

Further, we compare the output powers for different values of N. According to the study of Georges *et al* [48], the output power of the synchronized SHNOs depends on the

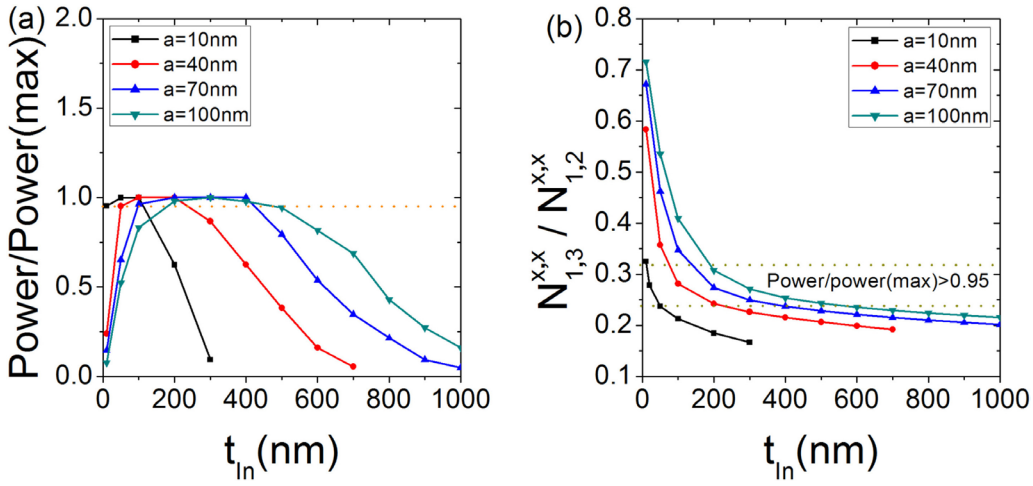

Figure 4. (a) Dependence of the normalized power as a function of t_{In} for different a, where the orange dotted line represents the boundary of power/power(max) = 0.95. For a smaller a, the maximum output power is observed at a smaller t_{In}. (b) Dependence of $N^{x,x}_{1,3}/N^{x,x}_{1,2}$ as a function of t_{In} for different a. $N^{x,x}_{1,3}/N^{x,x}_{1,2}$ decreases with the increase of t_{In} for all values of a.

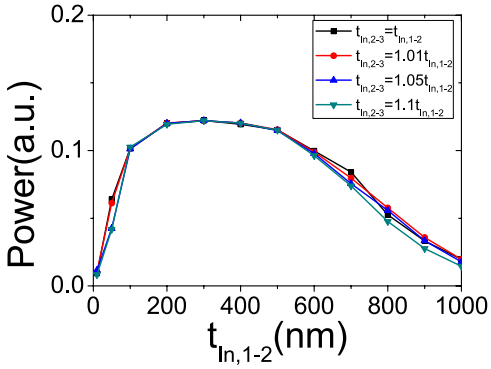

Figure 5. (a) Output power for different thicknesses of the insulator layers in different SHNOs.

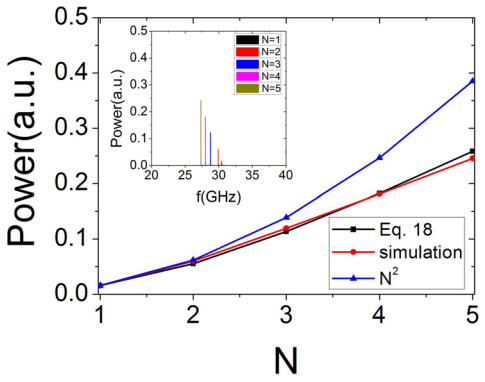

Figure 6. Output power as a function of N for $I_{\mathrm{dc}} = 24$ mA at t_{In} that corresponds to the maximum output power. The inset shows the output power in the frequency domain.

load resistance. For SHNOs connected in parallel, the output power can be expressed as:

$$P_{\mathrm{P}}(N) = \frac{R_{\mathrm{L}}N^2}{(NR_{\mathrm{L}}+R)^2}\Delta R^2_{\mathrm{osc}} I^2_{\mathrm{dc}}, \tag{16}$$

where $P_{\mathrm{P}}(N)$ is the output power of N SHNOs connected in parallel and ΔR_{osc} is the resistance variation of the SHNO. Equation (16) shows that the output power increases N^2 times in the N synchronized SHNOs connected in parallel only when $NR_{\mathrm{L}} << R$. Figure 6 shows the output powers of $N = 1, 2, 3, 4$, and 5 SHNOs for $I_{\mathrm{dc}} = 24.0$ mA, $2a = 200$ nm, $2b = 6$ μm, and $2c = 2$ nm at $t_{\mathrm{In,max}}$, where $t_{\mathrm{In,max}}$ is the thickness of the insulator that corresponds to the maximum output power for each N. The simulation results and those obtained using equation (16) are in a good agreement. As shown in figure 6, the output power at $N = 5$ is approximately 15.91 times larger than that at $N = 1$, as $R = 870$ Ω is not sufficiently large to satisfy the condition for the increase of the output power N^2 times upon the parallel connection of the SHNOs where $R = 870$ Ω is the resistance of the SHNO used in this study. The inset in figure 6 shows the output power for the different values of N in the frequency domain.

In addition, we calculate the thermal effect on the output power of the synchronized SHNOs. In the presence of thermal noise, the phase of SHNOs fluctuates and linewidth of the output power becomes broader [49]. We investigate the thermal effect on the output power, which depends on the phase difference between the SHNOs. The thermal effect in the nanomagnet is represented by the thermal field expressed as $\vec{H}_{\mathrm{th}} = \vec{G}\sqrt{2\alpha k_{\mathrm{B}}T/\gamma M_s V \Delta t}$, where $\vec{G}$ is a vector generated by a Gaussian random number generator, k_{B} is the Boltzmann constant, and Δt is a small amount of time corresponding to the time step in the numerical calculation. Figures 7(a) and (b) show the output powers of the synchronized SHNOs as a function of the distance between the SHNOs for $N = 2$ and $N = 3$, respectively, at $T = 0$ K, $T = 300$ K, and $T = 800$ K. These results reveal that the output power is not sensitive to temperature changes, which implies that the synchronized SHNOs are stable with respect to thermal fluctuations in the model [50].

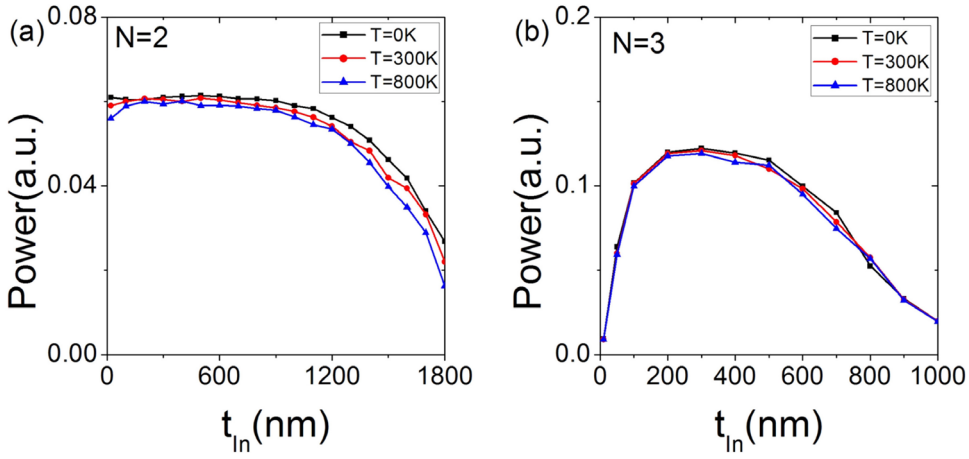

Figure 7. (a) Output power as a function of t_{In} for (a) $N = 2$ and (b) $N = 3$ at $T = 0$ K, $T = 300$ K, and $T = 800$ K.

4. Conclusion

By employing macrospin simulations, we investigated the synchronization between stacked SHNOs with magneto-dipolar interactions. In the SHNO system, the spin polarized current, which induced a magnetization precession in the ferromagnetic material through spin transfer torque, is generated by the SHE, while the magnetoresistance oscillations originated from the magnetization oscillation and AMR effect. We revealed that the output power increased in the synchronized state and depended on the phase difference between the SHNOs. When the output power was expressed as a function of t_{In}, $t_{\mathrm{In,max}}$ for $N = 2$ differed from that for $N = 3$. We observed that $t_{\mathrm{In,max}}$ for $N = 3$ could be varied by controlling the ratio between the coupling strength of the next-nearest neighbor and that of the nearest-neighbor, which was achieved by varying the SHNO's size as the cross-demagnetization tensor depended on the size of the SHNO. Furthermore, the output power increased with N; however, it did not increase to N^2 as in the parallel connection of the SHNOs, the output power could increase to N^2 only when $NR_{\mathrm{L}} \ll R$.

Acknowledgments

This work was supported in part by the MOTIE (10080725) and KSRC support program for the development of the future semiconductor device, and in part by BK21 plus in Korea Advanced Institute of Science and Technology (KAIST).

ORCID iDs

Kang Doo Hyung https://orcid.org/0000-0002-7858-3731

References

[1] Kawahara T, Ito K, Takemura R and Ohno H 2012 *Microelectron. Reliab.* **52** 613
[2] Khvalkovskiy A V *et al* 2013 *J. Phys. D: Appl. Phys.* **46** 074001
[3] Slonczewski K C 1996 *J. Magn. Magn. Mater.* **159** L1
[4] Berger L 1996 *Phys. Rev.* B **54** 9353
[5] Tsoi M, Jansen A G M, Bass J, Chiang W, Seck M, Tsoi V and Wyder P 1998 *Phys. Rev. Lett.* **80** 4281
[6] Katine J A, Albert F J, Buhrman R A, Myers E B and Ralph D C 2000 *Phys. Rev. Lett.* **84** 3149
[7] Grollier J, Cros V, Hamzic A, George J M, Jaffrès H and Fert A 2001 *Appl. Phys. Lett.* **78** 3663
[8] Zhang S, Levy P M and Fert A 2002 *Phys. Rev. Lett.* **88** 236601
[9] Barnas J, Fert A, Gmitra M, Weymann I and Dugaev V K 2005 *Phys. Rev.* B **72** 024426
[10] Mangin S, Ravelosona D, Katine J A, Carey M J, Terris B D and Fullerton E E 2006 *Nat. Mater.* **5** 210
[11] Tsoi M, Jansen A G M, Bass J, Chiang W, Tsoi V and Wyder P 2000 *Nature* **406** 46
[12] Fuchs G D, Emley N C, Krivorotov I N, Braganca P M, Ryan E M, Kiselev S I, Sankey J C, Ralph D C and Buhrman R A 2004 *Appl. Phys. Lett.* **85** 1205
[13] Ralph D C and Stiles M D 2008 *J. Magn. Magn. Mater.* **320** 1190
[14] Kiselev S I, Sankey J C, Krivorotov I N, Emley N C, Schoelkopf R J, Buhrman R A and Ralph D C 2003 *Nature* **425** 380
[15] Rippard W H, Pufall M R, Kaka S, Russek S E and Silva T J 2004 *Phys. Rev. Lett.* **92** 027201
[16] Krivorotov I N, Emley N C, Sankey J C, Kiselev S I, Ralph D C and Buhrman R A 2005 *Science* **307** 228
[17] Pufall M R, Rippard W H, Kaka S, Silva T J and Russek S E 2005 *Appl. Phys. Lett.* **86** 082506
[18] Slavin A N and Kabos P 2005 *IEEE Trans. Magn.* **41** 1264
[19] Krivorotov I N, Berkov D V, Gorn N L, Emley N C, Sankey J C, Ralph D C and Buhrman R A 2007 *Phys. Rev.* B **76** 024418
[20] Choi H S *et al* 2014 *Sci. Rep.* **4** 5486
[21] Liu L, Moriyama T, Ralph D C and Buhrman R A 2011 *Phys. Rev. Lett.* **106** 036601
[22] Liu L, Pai C, Ralph D C and Buhrman R A 2012 *Phys. Rev. Lett.* **109** 186602
[23] Demidov V E, Urazhdin S, Ulrichs H, Tiberkevich V, Slavin A N, Baither D, Schmitz G and Demokritov S O 2012 *Nat. Mater.* **11** 1028
[24] Liu R H, Lim W L and Urazhdin S 2013 *Phys. Rev. Lett.* **110** 147601
[25] Demidov V E, Urazhdin S, Zholud A, Sadovnikov A V and Demokritov S O 2014 *Appl. Phys. Lett.* **105** 172410
[26] Duan Z, Smith A, Yang L, Youngblood B, Lindner J, Demidov V E, Demokritov S O and Krivorotov I N 2014 *Nat. Commun.* **5** 5616
[27] Yang L *et al* 2015 *Sci. Rep.* **5** 16942

[28] Ranjbar M *et al* 2014 *IEEE Magn. Lett.* **5** 3000504
[29] Chen T, Dumas R K, Eklund A, Muduli P K, Houshang A, Awad A A, Dürrenfeld P, Malm B G, Rusu A and Åkerman J J 2016 *Proc. IEEE* **104** 1919
[30] Siracusano G, Tomasello R, Puliafito V, Giordano A, Azzerboni B, La Corte A, Carpentieri M and Finocchio G 2015 *J. Appl. Phys.* **117** 17E504
[31] Grollier J, Cros V and Fert A 2006 *Phys. Rev.* B **73** 060409
[32] Kaka S, Pufall M R, Rippard W H, Silva T J, Russek S E and Katine J A 2005 *Nature* **437** 389
[33] Mancoff F B, Rizzo N D, Engel B N and Tehrani S 2005 *Nature* **437** 393
[34] Slavin A N and Tiberkevich V 2009 *IEEE Trans. Magn.* **45** 1875
[35] Persson J, Zhou Y and Åkerman J 2007 *J. Appl. Phys.* **101** 09A503
[36] Zhou Y, Bonetti S, Persson J and Åkerman J 2009 *IEEE Trans. Magn.* **45** 2421
[37] Chen H, Lee C, Wu J, Horng L, Chang C and Chang J 2014 *J. Appl. Phys.* **115** 134306
[38] Puliafito V, Consolo G, Lopez-Diaz L and Azzerboni B 2014 *Physica* B **435** 44
[39] Chen H, Lee C, Zhang Z, Liu Y, Wu J, Horng L and Chang C 2016 *Phys. Rev.* B **93** 224410
[40] Fukushima H, Nakatani Y and Hayashi N 1998 *IEEE Trans. Magn.* **34** 193
[41] Dmytriiev O, Meitzler T, Bankowski E, Slavin A N and Tiberkevich V 2010 *J. Phys.: Condens. Matter* **22** 136001
[42] Smith A, Nielsen K K, Christensen D V, Bahl C R H, Bjørk R and Hattel J 2010 *J. Appl. Phys.* **107** 103910
[43] Akhieser A I, Bar'yakhtar V G and Peletminsky S V 1968 *Spin Waves* (Amsterdam: North-Holland)
[44] Kang D H, Park S and Shin M 2016 *IEEE Trans. Magn.* **52** 1400606
[45] Joseph I and Schlomann E 1965 *J. Appl. Phys.* **36** 1579
[46] Manzin A, Nabaei V, Corte-León H, Kazakova O, Krzysteczko P and Schumacher H W 2014 *IEEE Trans. Magn.* **50** 7100204
[47] Elyasi M, Bhatia C S and Yang H 2015 *J. Appl. Phys.* **117** 063907
[48] Georges B, Grollier J, Cros V and Fert A 2008 *Appl. Phys. Lett.* **92** 232504
[49] Taniguchi T 2014 *Appl. Phys. Express* **7** 053004
[50] d'Aquino M, Serpico C, Bonin R, Bertotti G and Mayergoyz I D 2010 *Phys. Rev.* B **82** 064415